DRP scheme, the advantage of the optimized upwind DRP scheme is that it automatically damps out the spurious short waves while retaining the DRP property in the scheme. The dissipation error is also minimal due to the optimization process. The results in Figs. 1a and 1b indicate that the optimized fourth-order upwind DRP scheme with $N=4$ and $M=2$ has much less dissipation error than that of the standard sixth-order upwind scheme with $N=4$ and $M=2$ and can also resolve waves with higher wave numbers (short waves). The coefficients a_j for the preceding optimized upwind DRP scheme with $N=4$ and $M=2$, shown in Fig. 1, were obtained with $\lambda=0.0374$ and $\sigma=0.2675\pi$. They are $a_{-4}=1.61404967150957E-02$, $a_{-3}=-1.22821279019864E-01$, $a_{-2}=4.55332277706221E-01$, $a_{-1}=-1.24925958826149$, $a_0=5.01890438019346E-01$, $a_1=4.39932192729636E-01$, and $a_2=-4.12145378889463E-02$.

III. Results and Discussion

To verify the behavior of the optimized upwind DRP scheme developed in the preceding section, the scheme, combined with a fourth-order explicit time discretization, is applied to solve the first-order linear wave equation.

In case 1, the half-period sine function is

$$u(x,0)=0, \qquad 0\le x\le 50$$

$$u(x,0)=100(\sin\{\pi[(x-50)/b]\}), \qquad 50\le x\le 50+b$$

$$u(x,0)=0, \qquad 50+b\le x\le 300$$

where b is proportional to the width of the wave.

In case 2, the discontinuous initial waveform is

$$u(x,0)=0, \qquad 0\le x\le 50$$

$$u(x,0)=100.0, \qquad 50\le x\le 110$$

$$u(x,0)=0, \qquad 110\le x\le 300$$

A. Comparisons with the Standard Sixth-Order Upwind Scheme

The first-order linear wave equation is solved for case 1 with $b=60$. Figures 2a and 2b give a comparison between the exact solutions and the numerical solutions for the optimized fourth-order upwind DRP scheme and the standard sixth-order upwind scheme, respectively. The computational domain is given as $0\le x\le 300$, and a mesh of spacing $\Delta x=3$ is chosen. Excellent agreement between the computed solutions of the optimized upwind DRP scheme and the exact solutions is shown for different times, $500\Delta t$ and $4000\Delta t$, where Δt is 0.0001. For the standard sixth-order scheme, however, the phase error increases as the time progresses. As we decrease the value of b, which is known to be proportional to the width of the wave, to 10, mesh spacing Δx has to be decreased to unity. The results shown in Figs. 3a and 3b indicate that for short waves the optimized upwind DRP scheme, due to the DRP property in the scheme, gives good velocity waveform. However, the dispersive error increases for the standard sixth-order upwind scheme, and the solution of the scheme is totally dispersed at the time $4000\Delta t$.

B. Comparisons with the Central DRP Scheme

To compare the performance of the optimized fourth-order upwind DRP with that of the fourth-order central DRP schemes, the first-order linear wave equation is solved for a discontinuous initial waveform (case 2) with a grid of spacing $\Delta x=0.5$. Figures 4a and 4b show the computed waveform at times $5000\Delta t$ and $50{,}000\Delta t$ by the central DRP scheme, where Δt is 0.00001. As we can see, the solution quality degrades by the presence of numerous fine-scale oscillations. The dispersive waves can also be seen superimposed on the main wave pulse. An artificial selective damping is needed to remove these pollutants of computational acoustics.[2,3] In contrast to the central DRP scheme, the results shown in Figs. 4c and 4d indicate that the solution of the optimized upwind DRP scheme has fewer oscillations and most of the spurious waves are automatically damped out due to the inherent viscosity in the scheme. Also, the dissipation error of the optimized upwind DRP scheme is minimum because the imaginary part of the integrated error E is minimized for a wide range of wave numbers.

IV. Conclusions

The optimized upwind DRP scheme is developed and validated. Results from the optimized fourth-order upwind DRP scheme show that numerical solutions of the scheme have much smaller dispersive and dissipation errors and can resolve waves with much shorter wavelengths than that of the standard sixth-order upwind scheme. Compared with the central DRP scheme, the advantage of the optimized upwind DRP scheme is that it removes most of the numerical contaminants of computational acoustics automatically due to the inherent viscosity in the scheme. The quality of numerical solutions is improved by the optimized upwind DRP scheme without adding artificial selective damping terms in finite difference equations.

Acknowledgment

We would like to acknowledge C. K. W. Tam for his helpful comments.

References

[1] Zingg, D. W., "A Review of High-Order and Optimized Finite-Difference Methods for Simulating Linear Wave Phenomena," AIAA Paper 97-2088, June 1997.

[2] Hardin, J. C., Ristorcelli, J. R., and Tam, C. K. W., *ICASE/LaRC Workshop on Benchmark Problems in Computational Aeroacoustics*, NASA CP-3300, 1995.

[3] Tam, C. K. W., Webb, J. C., and Dong, Z., "A Study of the Short Wave Components in Computational Acoustics," *Journal of Computational Acoustics*, Vol. 1, No. 1, 1993, pp. 1–30.

[4] Tam, C. K. W., and Webb, J. C., "Dispersion-Relation-Preserving Schemes for Computational Acoustics," *Journal of Computational Physics*, Vol. 107, No. 2, 1993, pp. 262–281.

[5] Li, Y., "Wavenumber-Extended High-Order Upwind-Biased Finite-Difference Schemes for Convective Scalar Transport," *Journal of Computational Physics*, Vol. 133, 1997, pp. 235–255.

D. S. McRae
Associate Editor

Finite Element and Dynamic Stiffness Methods Compared for Modal Analysis of Composite Wings

Mark Lillico* and Richard Butler†
University of Bath, Bath BA2 7AY, England, United Kingdom

Introduction

THE aim of the research, which is partly described in this Note, is to develop a design tool[1,2] for use by engineers involved in the conceptual design of wing structures. During the conceptual stage, there is only a limited amount of design information available, making the generation of complex three-dimensional finite element (FE) models difficult. There is also a need to examine numerous design configurations quickly. Therefore, it is important to have a tool that is accurate, efficient, quick to use, and simple, i.e., has a small number of design variables and a sufficient number of critical constraints. Also, because changes made late in the design process are expensive to carry out, it is important to include the effect of constraints that often are neglected at the conceptual stage, e.g., flutter. For these reasons, a one-dimensional dynamic stiffness method (DSM)[3] model has been used instead of a three-dimensional finite element method (FEM) model to find the normal modes of the wing. In previous work, it has been shown, by both experimental and FEM analysis, that the DSM can be used to accurately predict the normal modes

Received Dec. 16, 1997; revision received Aug. 8, 1998; accepted for publication Aug. 19, 1998.

*Research Assistant, Department of Mechanical Engineering.
†Lecturer in Aircraft Structures, Department of Mechanical Engineering.

Table 1 Natural frequencies of initial and final designs

	Initial design[a]			Final design[a]		
Mode	FE, Hz	DSM, Hz	% Difference	FE, Hz	DSM, Hz	% Difference
1	6.4B	6.2B	−3	6.5B	6.1B	−6
2	9.2B	10.2B	+10	11.4B	10.9B	−5
3	23.0B	23.9B	+4	19.7B	18.4B	−7
4	48.0B	52.5B	+9	35.9B/T	38.6B/T	+7
5	60.1T	62.8T	+4	41.0T	42.8T	+4
6	83.8B	96.7B	+13	59.0B	69.2B	+15
7	114.3T	123.1T	+7	62.2B	83.2T	——
8	125.4B/T	132.7T	+6	82.4T	98.7T	——

[a]B denotes a bending mode, and T denotes a torsional mode.

of composite plates.[4] The aim of this Note is to extend this work by comparing the one-dimensional DSM and three-dimensional FEM modal analysis of a composite wing box. The initial and optimum designs of a previously presented optimization problem[2] are used as example problems.

A full description of the external geometry, laminate layer thickness distribution, and position of the spars and engine for both wing designs is given in Ref. 2. Briefly, the initial wing design, which had a mass of 301 kg and a flutter speed of 368 m/s, was optimized for minimum mass subject to constraints on material stress and a minimum acceptable flutter speed of 270 m/s. The final design had a mass of 184 kg and a flutter speed of 270 m/s. (The flutter speed constraint has to be imposed during optimization, despite the fact that the initial design meets the requirement, because without it there would be no guarantee that the optimum design would satisfy the requirement.)

DSM Wing Model

An important feature of the DSM is the assumption of a continuous distribution of rigidity and mass, thus allowing for an infinite number of degrees of freedom. In constrast, the FEM discretizes the rigidity and mass distributions to nodal points and uses a finite number of degrees of freedom and hence can find a solution only for a finite number of modes, which are of limited accuracy for the higher-order modes. The DSM wing models therefore used only 10 uniform box beam elements, each 1.28 m long. The spar and skin laminates had a layup of $[90/-30/30/0]_S$, and the span-wise layer thickness distribution was modeled using a quadratic equation. The optimized design had unbalanced ±30-deg layers and therefore had coupled bending-torsional rigidity. The mass of the ribs and nonstructural components was accounted for by two spanwise distributed masses, one at the center of the wing box and the other at 80% chord. A preprocessor is used to calculate the cross-sectional properties (bending rigidity, torsional rigidity, coupled rigidity, mass, inertia, and distance between mass and elastic axes) of each element to be used in the DSM analysis.

FEM Wing Model

FE modal analysis was carried out using ANSYS.[5] Both designs were modeled as continuously tapering boxes (Fig. 1), which is more realistic than the DSM models. The composite wing box was meshed using eight-noded SHELL91 (Ref. 5) elements, and the box was divided into 10 bays, each 1.28 m long, within which the thickness of each layer in the spar and skin laminates was the same as the layer thickness in the corresponding DSM element. Twenty MASS21 (Ref. 5) elements, with no inertia about their own c.g., were used to model the nonstructural masses. These were positioned at the midspan of each bay (Fig. 1) and were attached using BEAM4 (Ref. 5) elements with a cross-sectional area of 1×10^{-4} m^2 and a second moment of area of 8.333×10^{-10} m^4. Because the latter are not included in the DSM model, they were given a low density ($\rho = 0.1 \times 10^{-3}$ kg/m^3) and high elastic and shear moduli (E and $G = 0.1 \times 10^{17}$ N/m^2). The engine also was modeled using a MASS21 element, and inertia terms about its own c.g. were included.

To prevent a significant amount of cross-sectional deformation from occurring, 20 ribs were added at 0.64-m intervals along the span, using SHELL41 (Ref. 5) membrane shell elements. The thickness of the ribs varied linearly, from 1 mm at the tip to 3 mm at the root. They were constructed of an aluminum-like material ($E = 70 \times 10^9$ N/m^2, $G = 27 \times 10^9$ N/m^2, and $\nu = 0.3$). There was no need for ribs in the DSM model because of the beam-theory assumption of no cross-sectional deformation, and so they were given a density of only 0.1 kg/m^3.

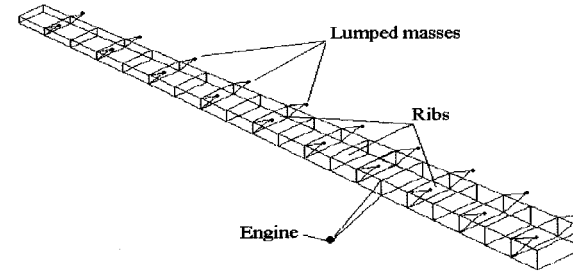

Fig. 1 Geometry of FEM wing model.

The FEM models for the initial and optimum designs consisted of 2070 and 1517 elements, respectively. To ensure that only overall modes were obtained and to reduce the analysis time, 60 master degrees of freedom were selected along each of the box edges.

Discussion of Results

The natural frequencies for both designs are compared in Table 1. For the initial design the natural frequencies given by both methods are within 15% of each other and within 5% for the fundamental bending and torsional modes. Except for the fundamental bending mode, the natural frequencies obtained by the FEM are lower than those predicted by the DSM. The mode shapes predicted by both DSM and FEM for the first seven modes, although not shown here, are similar. The DSM analysis predicts that mode 8 is predominately a torsional mode with only a little bending displacement, whereas the FEM analysis predicts a mode that has a considerable amount of both bending and torsional displacement, although bending is more significant.

For the optimum design, the natural frequencies predicted by both methods for the first five modes were within 10% of each other. For this design, the frequencies for the first three modes predicted by FEM were greater than those predicted by the DSM. It is thought that the differences between the predicted natural frequencies for both designs is partly due to differences in inertia caused by modeling the nonstructural masses as discrete lumps in the FEM models rather than as continuous distributions as in the DSM models. The mode shapes predicted by both methods are similar for the first five modes (Fig. 2). Although both methods agree on the frequency of the second torsional mode, the DSM analysis predicts that it should be mode 7, whereas the FEM analysis predicts that it should be mode 8 because of the presence of an additional bending mode. With the exception of the FEM's fundamental bending and second bending modes and the DSM's second bending mode, the frequencies of all modes are reduced during optimization.

For the initial wing design, modal analysis using FEM took 22 min and 23 s to obtain a solution for the first seven modes, whereas using the DSM, the solution was obtained in only 2 s. These times

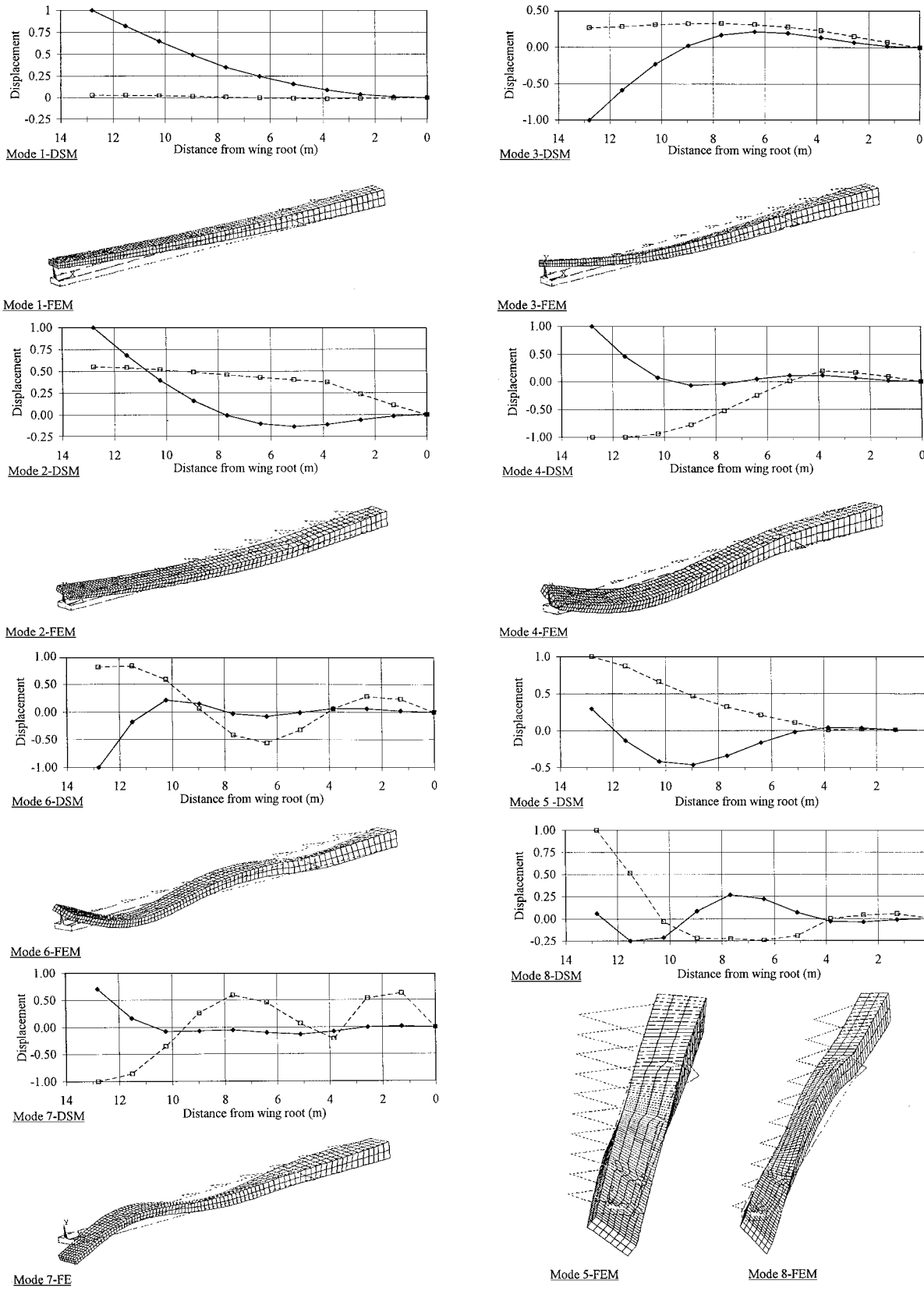

Fig. 2 DSM and FEM mode shapes for optimum design. For the DSM results, a solid line denotes bending displacement and a dotted line denotes torsional displacement.

were obtained on a Silicon Graphic Indy 150 MHz workstation. This substantial time difference will have a considerable effect on the time taken to obtain an optimum solution because, every time the flutter speed of a wing is required during optimization, modal analysis will need to be carried out. This is especially true if a gradient-based optimization method is used, where, when needed, the sensitivity of the flutter speed to a change in each design variable may be calculated using finite differencing.

Conclusions

The use of the DSM to predict the modal behavior of a wing has been validated against FEM. It also has been shown that the modal behavior of a relatively complex three-dimensional structure can be modeled satisfactorily using a one-dimensional DSM model and that a solution can be obtained in substantially less time using the DSM compared with the FEM. Thus, the former is more suitable for use at the conceptual design stage. Also, it has been illustrated

that, as a result of optimization, the design has not been moved into an area of the design space where the solutions obtained by FE and DSM cease to be comparable. Finally, the use of the simpler DSM model allows an understanding of the way in which the properties of the wing, such as bending rigidity and torsional rigidity, vary during optimization because these are obtained explicitly as part of the analysis process.

Acknowledgments

The authors would like to thank J. R. Banerjee at City University, London; the Engineering and Physical Sciences Research Council; and British Aerospace Airbus Ltd. for the assistance that they have given during this work.

References

[1]Lillico, M., Butler, R., Guo, S. J., and Banerjee, J. R., "Aeroelastic Optimisation of Composite Wings Using the Dynamic Stiffness Method," *Aeronautical Journal*, Vol. 101, No. 1002, 1997, pp. 77–86.

[2]Lillico, M., Butler, R., and Holden, M., "Conceptual Design Optimization of Composite Wings with Aeroelastic and Strength Constraints," *Proceedings of the AIAA/NASA/USAF 6th Symposium on Multidisciplinary Analysis and Optimization* (Bellevue, WA), AIAA, Reston, VA, 1996, pp. 191–200.

[3]Banerjee, J. R., and Williams, F. W., "Free Vibration of Composite Beams—An Exact Method Using Symbolic Computation," *Journal of Aircraft*, Vol. 32, No. 3, 1995, pp. 636–642.

[4]Taylor, J. M., and Butler, R., "Optimum Design and Validation of Flat Composite Beams Subject to Frequency Constraints," *AIAA Journal*, Vol. 35, No. 3, 1997, pp. 540–545.

[5]*ANSYS User's Manual*, Version 5.0, Swanson Analysis Systems Inc., Houston, PA, 1992.

A. M. Waas
Associate Editor